Selective aqueous phase hydrogenation of xylose to xylitol over SiO2-supported Ni and Ni-Fe catalysts: Benefits of promotion by Fe

Achraf Sadier, Dichao Shi, Anne-Sophie Mamede, Sébastien Paul, Eric Marceau, Robert Wojcieszak

Selective aqueous phase hydrogenation of xylose to xylitol over SiO_2-supported Ni and Ni-Fe catalysts: Benefits of promotion by Fe

Achraf Sadier, Dichao Shi, Anne-Sophie Mamede, Sébastien Paul, Eric Marceau*, Robert Wojcieszak*

Univ. Lille, CNRS, Centrale Lille, Univ. Artois, UMR 8181 – UCCS – Unité de Catalyse et Chimie du Solide, F-59000 Lille, France

Abstract: A monometallic Ni and a bimetallic Ni-Fe catalyst were used in the aqueous phase hydrogenation of xylose in batch conditions (T = 50 - 150 °C, P_{H2} = 10 - 30 bar, xylose mass fraction in water = 3.7 - 11.0 wt.%) to evidence the benefits of promoting Ni by Fe. The activity of the catalysts increased with temperature, but a temperature of 80 °C allowed minimizing nickel leaching at full conversion. The presence of reduced Fe at the surface of the bimetallic nanoparticles increased both the first-order apparent rate constant and the adsorption constant of xylose. The catalytic activity of Ni/SiO_2 strongly declined and no deactivation was found for the Ni-Fe catalyst. A restructuring of the bimetallic nanoparticles took place, as the size of the metal particles and the Fe proportion in the surface layers increased, suggesting a flattening and coalescing of the particles over the silica surface.

Introduction

While the industrial production of a wide range of raw chemicals has heavily relied on petroleum,[1] the forecast dwindling of fossil resources is currently shifting the synthesis of high added-value products toward the transformation of renewable lignocellulosic biomass.[2–5] Xylan-rich hemicellulose is a source of xylose, which can be converted into xylitol by direct hydrogenation (Scheme 1).[6] According to the US Department of Energy (DOE), xylitol ranks among the twelve most relevant platform molecules issued from biomass.[7] Its anti-carcinogenic and high sweetening properties make it a valuable candidate for applications in the food, cosmetics, and pharmaceutical industries.[8–13] Daily use products such as chewing gums, chocolates, toothpastes, mouth fresheners, and oral hygiene products contain xylitol.[6,14] The estimated global market of xylitol has increased from 161 thousand metric tons in 2013 to 242 thousand metric tons in 2020.[15]

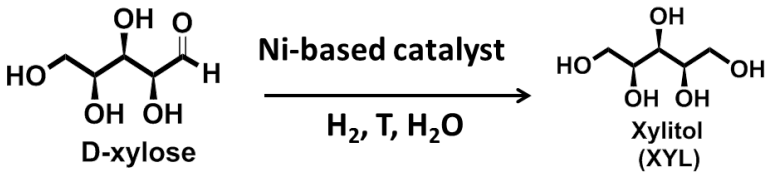

Scheme 1: Hydrogenation of xylose to xylitol.

Various noble metals, such as Pt, Pd, and Ru, have been considered for the catalytic hydrogenation of xylose to xylitol. Ru-based catalysts have appeared as the most efficient in terms of activity and stability in water,[16–18] with ruthenium up to 50 times more active than nickel.[19] Despite their high performance, the major drawbacks of noble metals in terms of sustainability and cost make it attractive to search for alternative non-noble metals. The use of Co and Cu has been reported in a few recent occurrences. Audemar *et al*. investigated the hydrogenation of xylose (5 wt.% in water) over a Co(10 wt.%)/SiO_2 catalyst under 50 bar H_2 at 140 °C for 2 h. Selectivity to xylitol remained almost unchanged after three cycles (~ 85%; side products: D-arabinitol, furfuryl alcohol, D-xylulose), but the catalytic conversion decreased from 97 up to 58% for the fourth cycle.[20] In another work, the one-pot cascade

conversion of xylose to furfuryl alcohol over a Cu/SBA-15-SO_3H catalyst was studied, and xylitol was a by-product of reaction (10% yield, against 62.6% for furfuryl alcohol).[21]

More references are available about nickel, with commercial Raney® Ni as the benchmark catalyst, and a high selectivity to xylitol has been reported.[9,22–25] The hydrogenation of concentrated aqueous solutions of xylose (20-60 wt.%) has been extensively studied in batch-type reactors under 35-60 bar H_2 in the temperature range 80-130 °C. The selectivity to xylitol at high conversion was higher than 95%. Nevertheless, the deposition of organic by-products makes Raney® Ni susceptible to deactivation upon recycling,[26–28] and the leaching of nickel requires the addition of costly purification and separation steps, especially for the food and pharmaceutical industries.[22,29,30]

On the other hand, the addition of a metallic promoter has been shown to enhance the catalytic performances of Ni in the hydro-conversion of other saccharides, such as glucose and cellulose.[28,31–35] Gallezot *et al*. studied the addition of promoters to Raney® Ni, such as Cr, Mo, Sn and Fe, in the aqueous phase hydrogenation of glucose (40 wt.% in a 10% solution of acetic acid) at 130 °C under 50 bar H_2. The addition of Mo and Cr increased the rate of glucose hydrogenation up to six times.[28] At 245 °C under 60 bar H_2, 4%Ni-1%Ir/mesoporous carbon was shown to perform the hydrolysis/hydrogenation of cellulose in a 1 wt.% solution.[32] On monometallic Ni, the hexitol yield (sorbitol + mannitol) decreased from 60 to 22% upon five cycles, due to agglomeration and leaching of Ni particles. On the other hand, the activity (100%) and yield to hexitols (60%) were maintained for four recycling tests with the Ni-Ir catalyst.[32] Finally, 17%Ni-1%Pt/ZSM-5 displayed a good stability in the aqueous phase hydrogenation of cellulose (3 wt.%) at 240 °C under 40 bar H_2 with a yield of hexitols that remained higher than 55% after the catalyst was reused four times.[33]

Only in a few instances have bimetallic Ni-based catalysts been applied to the hydrogenation of xylose. Ni/AC and Ni-Re/AC catalysts (n_{Ni}:n_{Re} = 1:1; AC: activated carbon) were investigated in a 4.8 wt.% xylose aqueous solution, at 140 °C, under 20 bar H_2. After 1 h, Ni/AC yielded 62.7% of xylitol at 70% conversion, and the addition of Re increased the activity, producing 98% of xylitol at 99% conversion.[31] Chieffi *et al.* have reported that xylose (0.1 mol.L^{-1} in water) was quantitatively hydrogenated into xylitol at 150 °C under 50 bar H_2, in a continuous process based on a 27wt.% Ni-20 wt.% Fe catalyst supported on

carbon, but no kinetic study was provided.[34] Indeed, compared with rhenium, Fe appears as a promising promoter of Ni due to its abundance and low cost.[36] The relevance of Fe as an efficient cost-effective promoter has been recently confirmed by a recent report on the hydrogenation of a 0.5 wt.% glucose aqueous solution at 140 °C, under 30 bar H_2, in the presence of Ni-Fe alloyed particles supported on carbon black (CB).[35] After 2 h, Ni/CB yielded 16.7% sorbitol at 33.1% glucose conversion, while the addition of Fe (atomic ratio of 1:1) increased the activity (70.4% conversion), producing 50% of sorbitol. The Ni-Fe alloy also exhibited advantages over monometallic Ni in terms of stability.

To our best knowledge, the benefit of using supported Ni-Fe-based catalysts with respect to Ni catalysts has never been investigated in detail for the aqueous phase hydrogenation of xylose. In the present work, a monometallic Ni catalyst and a bimetallic Ni-Fe catalyst, both prepared by deposition-precipitation and featuring the same structural characteristics in terms of particle size and size distribution, are compared in batch conditions, in order to identify the influence of the reaction parameters (*e.g.,* temperature, xylose concentration, hydrogen pressure) on their activity, selectivity and stability, and to evidence the advantages brought by the Fe promotion.

Experimental section

Catalysts preparation

Sipernat-50 silica (Degussa; surface area, 400m^2 g^{-1}, pore volume, 1.4 cm^3 g^{-1}), iron (II) sulfate heptahydrate (Alfa Aesar, 98%), nickel (II) sulfate hexahydrate (Aldrich, 99%), sulfuric acid (Alfa Aesar, 93–98%) and urea (Alfa Aesar, 99–100%) were used for the synthesis of the catalysts without further purification.

Two catalysts, monometallic Ni_{100}/SiO_2 and bimetallic $Ni_{62}Fe_{38}/SiO_2$ (where the figures represent the molar proportions of the two metals in the reduced nanoparticles), were prepared by deposition-precipitation with urea (DPU) following a protocol of deposition previously reported; in this former work, the bimetallic catalyst was found to exhibit superior properties in the selective hydrogenation of furfural to furfuryl alcohol.[37] Reduction of the solids recovered after DPU was performed at 700 °C for 2 h under 10% H_2/Ar (100 mL min^{-1}, heating ramp 5 °C min^{-1}), in order to completely reduce Ni and Fe. It was formerly shown by *in situ* X-ray absorption and Mössbauer spectroscopies applied to the bimetallic catalyst that the reduction of

Ni^{2+} to Ni(0) preceded the reduction of Fe^{2+} ions to Fe(0), with a progressive insertion of Fe atoms into the *fcc* structure of the alloyed particles, ending with an Fe-enriched shell surrounding a Ni-enriched core. After reduction at 700 °C, the bimetallic particles were homogeneous in size on the two catalysts (average size: 5.4 nm; standard deviation: 1.3 nm), and homogeneous in composition on the bimetallic catalyst (standard deviation of composition: 8 Fe at %). The dispersion of the metallic nanoparticles, based on TEM measurements, was calculated as 20% for both catalysts. Ni_{100}/SiO_2 exhibited a 40 wt.% loading of Ni, while for $Ni_{62}Fe_{38}/SiO_2$, the Ni and Fe loadings were 26 and 16 wt.%, respectively.[37]

A Cu_{100}/SiO_2 (40 Cu wt.%) catalyst was also prepared by the same method for the sake of comparison, using a solution of 0.28 mol L^{-1} Cu(II) nitrate for DPU (copper (II) nitrate trihydrate, Alfa Aesar, 98%). This catalyst was active in the hydrogenation of xylose to xylitol, but considerably less than the Ni_{100}/SiO_2 catalyst. Results are presented for information in the Supplementary material (**Erreur ! Source du renvoi introuvable.**-S4).

Characterization of catalysts and solutions

The elemental analysis of Ni, Fe, and Si was performed on the prepared catalysts, and on the liquid solution at the end of reaction, by Inductively Coupled Plasma Optical Emission Spectrometry (ICP-OES), using an Agilent 720-ES ICP-OES equipment combined with a Vulcan 42S automated digestion system.

TGA analysis was carried out under air (flow rate 100 $mL.min^{-1}$). The samples were heated from room temperature to 800 °C at a temperature ramp of 3 $°C.min^{-1}$ in a Labsys TGA-DTA 1,600 apparatus.

Powder X-ray diffraction patterns (XRD) of the catalysts were recorded in ambient conditions using a Bruker AXS D8 Advance diffractometer equipped with a nickel filter, a copper tube ($\lambda K\alpha$ (Cu) = 1.54184 Å) and a multi-channel fast detector. Samples were scanned at 0.014 ° s^{-1} over the range $5 \leq 2\theta \leq 80°$.

Transmission electron microscopy (TEM) images were obtained by using a Tecnai G2 20 microscope equipped with a LaB_6 filament and operating at 200 kV, also equipped with an EDX detector and a GATAN CCD camera (Orius SC1000A). The images have been acquired in the parallel beam TEM mode.

The low-energy ion scattering (LEIS) analyses were performed on a Qtac100 spectrometer (IONTOF GmbH). A 5 keV Ne^+ beam at normal incidence was selected for quantitative Fe and Ni analysis (1 nA beam current).[38] Prior to LEIS measurements, the samples were treated *in situ* under pure hydrogen at 400°C for 2h in a dedicated cell coupled to the spectrometer, allowing transfer under UHV without air contamination. Attention was given to the experimental parameters (analyzed area, acquisition time), so that the initial ionic dose per spectrum (4.8 x 10^{13} ions.cm^{-2}) did not exceed 5% of a monolayer to analyze the outermost atomic layer only. The ionic dose per spectrum was then increased to 1.2 x 10^{15} ions.cm^{-2} in order to analyze the atomic composition of the sub-surface. The data were processed using the SurfaceLab software from the same manufacturer. The ratio of the sensitivity factors $\eta(Fe)/\eta(Ni)$ used for the relative quantification of the two metals was previously evaluated using Fe_2O_3 and NiO reference powders and found to be equal to 0.91. The methodology is described elsewhere.[39,40] Because the Fe and Ni signals are separated by a theoretical energy of 68 eV only, the LEIS signal was decomposed using the two experimental lineshapes provided by the Fe and Ni peaks of the Fe_2O_3 and NiO reference materials, respectively, in order to take the isotopic distribution of each metal into account.

Catalytic testing

The hydrogenation of D-xylose (Fisher, 99%) was carried out in a 30 mL batch Hastelloy Parr autoclave. The catalysts formerly reduced at 700°C and stored in air were activated under pure hydrogen (3 bar) at 400 °C for 2 h using a Screening Pressure Reactor (SPR) from Unchained Labs, and collected inside a glove box to avoid the re-oxidation of the metals. 24 mL of xylose aqueous solution (concentrations 0.26–0.84 mol.L^{-1}, corresponding to mass fractions 3.7-11.0 wt.%) and 108 mg of catalyst were loaded into the reactor without exposure to air. After sealing, the autoclave was purged 3 times with H_2, pressurized with H_2 to the required pressure (P_{H2} =10-30 bar), and finally heated to the reaction temperature (T = 50-150 °C) under stirring (600 rpm). During the experiment, liquid samples were collected to follow the kinetics of the reaction. At the end of the reaction, H_2 pressure was released, the reactor was cooled, and the catalyst was collected by centrifugation. At the end of each reaction, the aqueous solution was analyzed by ICP to detect the leaching of metals expressed in ppm. A blank test was performed without catalyst and no conversion of xylose was observed.

The reaction products were analyzed by High Performance Liquid Chromatography (HPLC, Waters 2410 RJ) equipped with RI and UV detectors and a Rezex ROA–organic Acid H^+ column (Ø 7.8 mm x 300 mm) at 25 °C. Diluted H_2SO_4 (5 mmol.L^{-1}, 0.6 mL.min^{-1}) was used as the mobile phase. The products were identified by their retention times compared to available standards that were also used to determine the response factors. The effective separation of xylose and xylitol is illustrated on **Erreur ! Source du renvoi introuvable.**.

The conversion of xylose at time t was calculated was calculated from equation (1):

$$Conversion_t(\%) = \frac{C_0^{xylose} - C_t^{xylose}}{C_0^{xylose}} \times 100 \qquad (1)$$

where C_0^{xylose} is the initial concentration of xylose and C_t^{xylose} is the concentration of xylose at time t. The carbon selectivity to xylitol was calculated using equation (2):

$$S_t^{xylitol}(\%) = \frac{C_t^{xylitol} \times 5}{(C_0^{xylose} - C_t^{xylose}) \times 5} \times 100 \qquad (2)$$

in which $C_t^{xylitol}$ is the concentration of xylitol at time t.

Kinetic studies were performed with identical masses of the monometallic and of the bimetallic catalysts. Normalization with respect to the particles surface area would not alter the comparison, given the similar dispersion and size distribution of the metal particles on the two catalysts. However, calculating rates normalized with respect to Ni only, or with respect to a single surface metal atom, would introduce biases, because the distribution of Ni through the alloyed Ni-Fe particles has been shown to be uneven,[37] and the definition and quantification of the active sites, which may involve both Fe and Ni at the surface of the bimetallic particles as will be discussed below, is not straightforward. It was thus preferred to compare the catalysts through kinetic models that would describe the evolution of xylose conversion with time, rather than calculating normalized rates with a doubt on the meaning of the normalization.

Results and discussion

Screening of experimental parameters: temperature and metal leaching

In a first set of experiments, the concentration of xylose in the aqueous solution was fixed to 0.26 mol.L^{-1} (3.7 wt.% in water), the pressure of H_2 was set to 20 bar, and the temperature of reaction was varied between 50 and 150 °C. The evolution of xylose concentration as a function of time is presented in Figure 1. At 50 °C, an almost full conversion could be attained, but only after 15 h. An increase of the reaction temperature significantly accelerated the reaction: for example, at 80 °C, a xylose conversion of 95% was obtained after 3 h using $Ni_{62}Fe_{38}/SiO_2$, whereas 4 h were needed to reach the same conversion using Ni_{100}/SiO_2. In the whole temperature range, and for both catalysts, the carbon balance was higher than 98%. The only detected product was xylitol (selectivity > 98%). No minor products were identified.

Plotting $\ln(C_0^{xylose}/C_t^{xylose})$ versus time showed that in a first approximation, the reaction could be modelled for all these experiments with a first-order kinetics with respect to xylose (**Erreur ! Source du renvoi introuvable.**). This is in agreement with analyses reported by other authors: Mikkola *et al.* found a pseudo-first order dependency with respect to xylose using Raney Ni- and Ru-based catalysts.[41,42] The values of the first-order apparent rate constants (k_{app}) at each temperature are reported in **Erreur ! Source du renvoi introuvable.**. Values of k_{app} are larger for the Ni-Fe catalyst up to 125 °C, but the gap narrows as the reaction temperature increases.

From the Arrhenius plot of $\ln(k_{app})$ versus 1/T(K) (**Erreur ! Source du renvoi introuvable.**), it was calculated that the apparent activation energy (Ea) was 42 and 38 kJ.mol^{-1} over Ni_{00}/SiO_2 and $Ni_{62}Fe_{38}/SiO_2$, respectively (**Erreur ! Source du renvoi introuvable.**). Values close to 50 kJ.mol^{-1} have been reported for Raney Ni and Ru-based catalysts.[41–43] However, some of these values are derived from kinetic modelling. They thus correspond to the activation energy of the assumed rate-determining step (reaction between adsorbed xylose and hydrogen atoms), whereas our calculations are based on the global apparent rate constants.

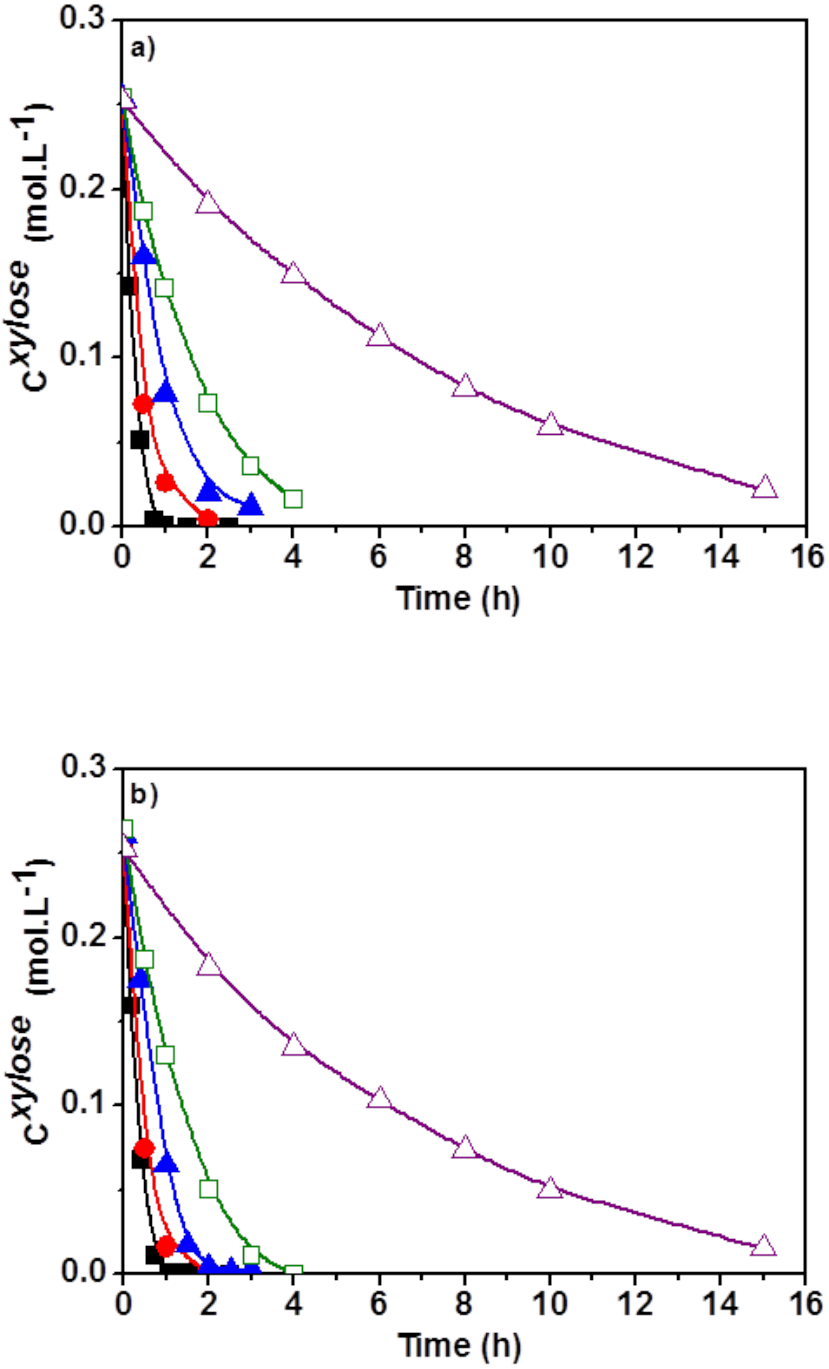

Figure 1: Effect of reaction temperature on temporal evolution of xylose concentration over a) Ni_{100}/SiO_2, b) $Ni_{62}Fe_{38}/SiO_2$ catalysts: (■) 150 °C; (●) 125 °C; (▲) 100 °C; (□) 80 °C; (△) 50 °C. Reaction conditions: 3.7 wt.% xylose, 20 bar H_2, 108 mg catalyst, $n_{xylose}/n_{Ni} = 9.7$, $n_{xylose}/n_{Ni+Fe} = 10.6$.

A first-order model thus fits our experimental measurements and are consistent with formerly reported data, though with possible discrepancies as far as activation energies are concerned. The limitations of this preliminary approach will be discussed in the next section.

The effect of reaction temperature on metal leaching measured by ICP in the recovered liquid phases at 95-100% conversion is presented in Figure 2a for the Ni catalyst and Figure 2b for the Ni-Fe catalyst. The scale for Si (blue circles) is to be read on the right-hand axis of the graphs. For the Ni catalyst, the concentrations of Ni and Si significantly decreased from 25 and 307 ppm, respectively, to 12 and 124 ppm, as the reaction temperature decreased from 150 to 80 °C. A similar trend was observed for Fe, Ni and Si for the $Ni_{62}Fe_{38}/SiO_2$ catalyst, but the leaching of Si was lower than for the Ni catalyst at high temperature. Ni leaching from the bimetallic catalyst was minimal at 80 °C (7 ppm). On the other hand, the leaching of Ni was more pronounced at 50 °C than at 80 °C. This can be related to the much longer reaction time needed to reach full conversion at this lower temperature.

It can be concluded from this screening of reaction parameters that for the two catalysts, a reaction temperature of 80 °C can be preferably selected to study the conversion of xylose to xylitol, as the reaction time to attain the full conversion of xylose is limited to a few hours, and metal leaching, especially that of Ni, is low. It was verified for the two catalysts that at 80 °C the initial reaction rate was proportional to the mass of catalyst up to 108 mg, allowing for a kinetic study in which the specificities of the more active Ni-Fe catalyst will be identified.

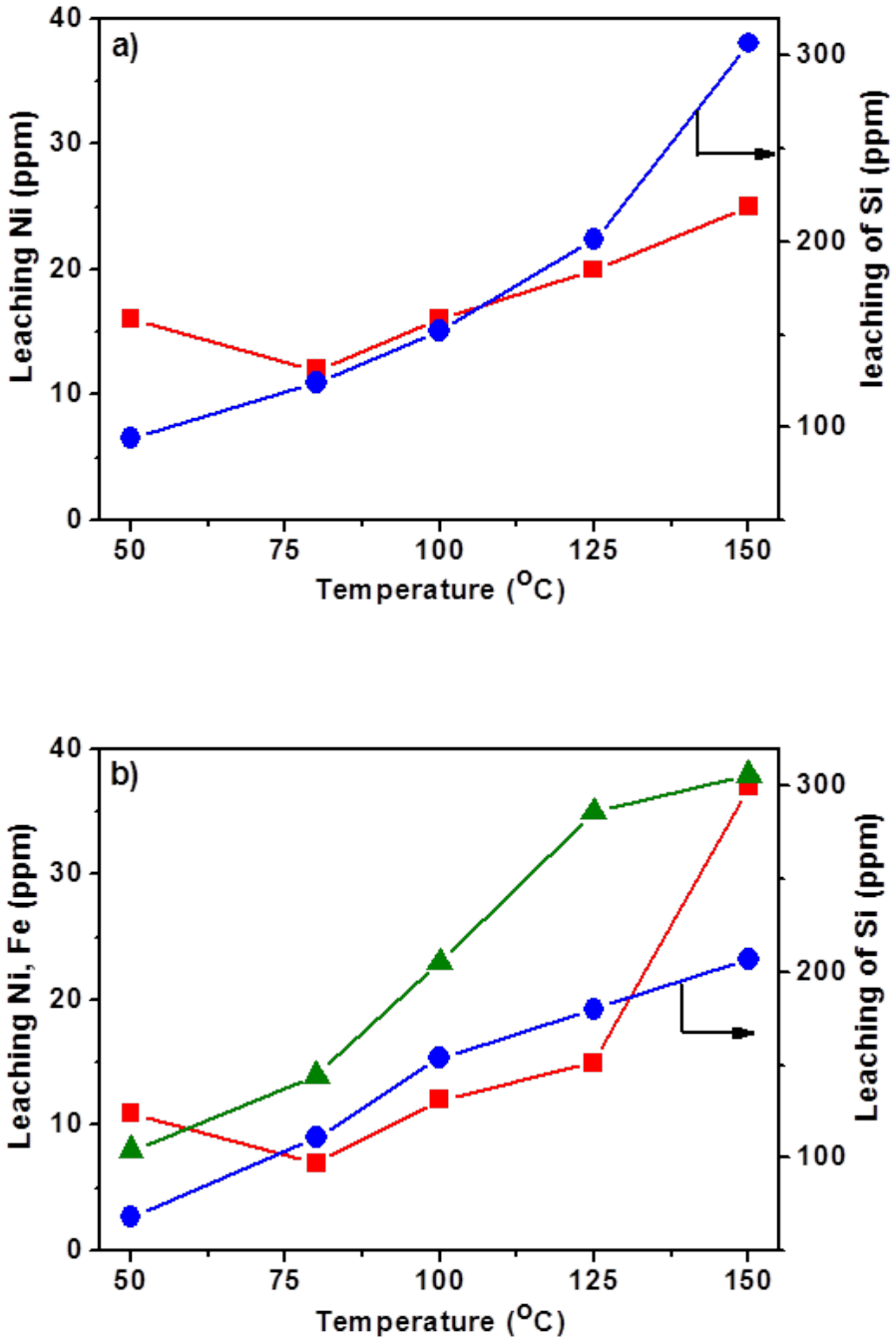

Figure 2: Effect of reaction temperature on metal leaching over a) Ni_{100}/SiO_2, b) $Ni_{62}Fe_{38}/SiO_2$ catalysts at full conversion of xylose. (■) Ni; (▲) Fe; (●) Si. Reaction conditions: 3.7 wt.% xylose, 20 bar H_2, 108 mg catalyst, $n_{xylose}/n_{Ni} = 9.7$, $n_{xylose}/n_{Ni+Fe} = 10.6$.

Effect of xylose concentration and hydrogen pressure

The effect of xylose concentration in the range 0.26-0.84 mol.L^{-1} (3.7-11.0 wt.%) was investigated at 80 °C, under 20 bar H_2. Xylose concentration was adjusted by varying the mass of xylose in a constant volume of water (24 mL).

The evolution of xylose concentration as a function of time is shown on Figure 3 (where symbols represent the experimental points and curves the model detailed below). The selectivity to xylitol remained higher than 98% in the whole range of xylose concentration, with a carbon balance higher than 98%. The values of the apparent rate constant (k_{app}) were first calculated using the simple first-order model described above. **Erreur ! Source du renvoi introuvable.** shows that k_{app} decreases strongly when the initial xylose concentration increases. This suggests that the first-order model is simplistic, and that xylose probably appears as an inhibitor in the rate law, as was the case in the model proposed by Pham *et al*.[41]

An alternative model involving an inhibiting term was thus tested for each catalyst at 80 °C, as described by equation (4):

$$\text{rate r} = \frac{\text{k} \times C^{xylose}}{1+\text{K}\times C^{xylose}} \qquad (4)$$

This model supposes: (i) an adsorption of xylose following a Langmuir isotherm based on an adsorption constant K, (ii) a concentration of H_2 imposed by the H_2 pressure in the reactor, that does not vary with time, and is included as a component of the rate constant k, (iii) no competitive adsorption between xylose and H_2. This is the main difference with the model from Pham *et al*., in which competitive adsorption between H_2 and xylose is assumed, though for quite higher pressure and temperature ranges (40-70 bar, 120-130 °C).[41]

For each catalyst, a plausible pair of k and K descriptors explaining the three evolutions of xylose concentration at 80 °C was determined by linear regression applied to 1/r plotted as a function of 1 / C^{xylose}(**Erreur ! Source du renvoi introuvable.**), leading for Ni_{00}/SiO_2 to k = 0.013 min^{-1} and K = 0.77 L.mol^{-1}, and for $Ni_{62}Fe_{38}/SiO_2$ to k = 0.020 min^{-1} and K = 2.40 L.mol^{-1}.

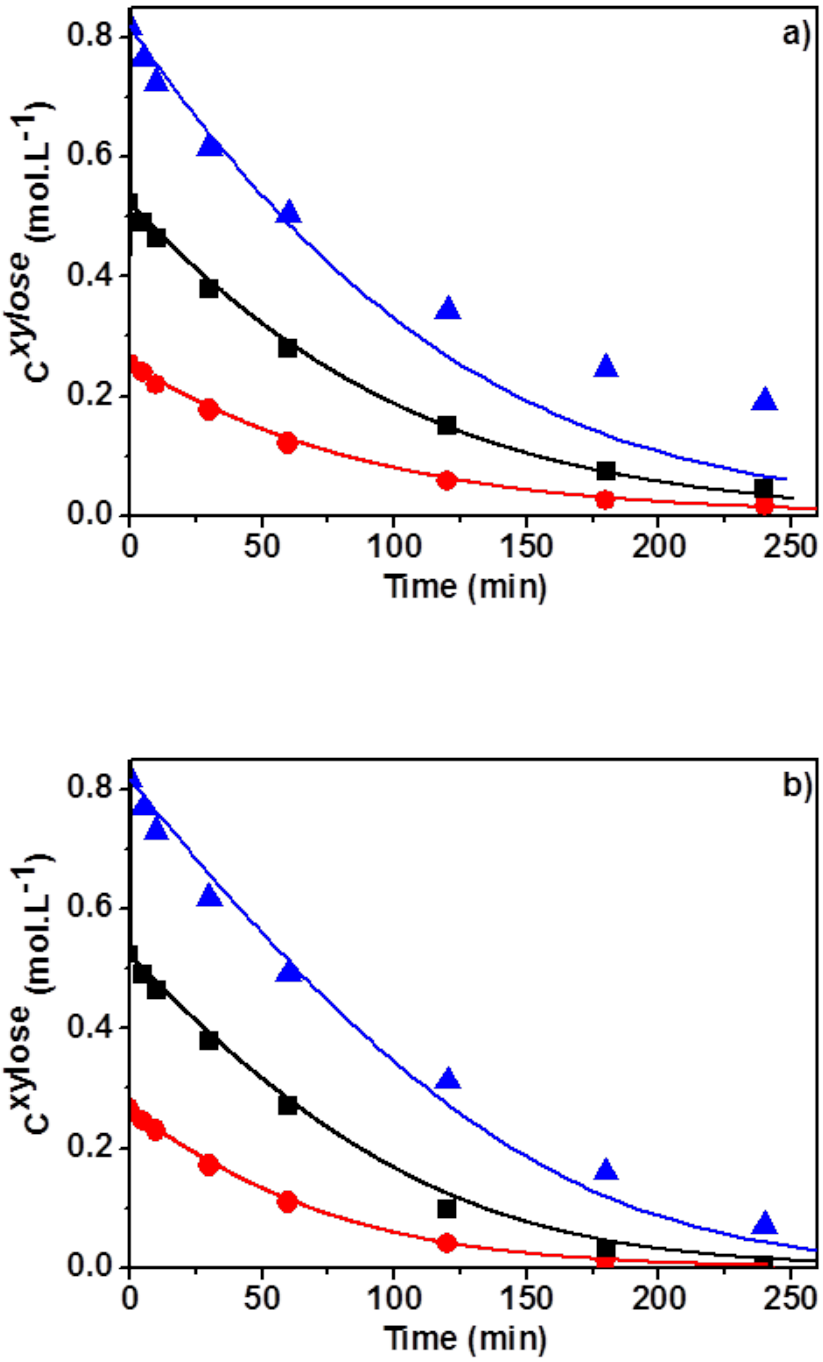

Figure 3: Evolution of xylose concentration as a function of time and initial xylose concentration over a) Ni_{100}/SiO_2 and b) $Ni_{62}Fe_{38}/SiO_2$ catalysts: (●) 3.7 wt.%; (■) 7.3 wt.%; (▲) 11.0 wt.%. Reaction conditions: 20 bar H_2, 80 °C, 108 mg catalyst. Curves are calculated using the model based on equation (5).

The agreement with the evolution of the experimental data was verified after integration of the rate law:

$$\ln\left(\frac{C0^{xylose}}{Ct^{xylose}}\right) + \mathrm{K}\left(C_0^{xylose} - C_t^{xylose}\right) = \mathrm{kt} \qquad (5)$$

Modelled curves are displayed on Figure 3 along with the experimental data. The fits between experimental data and model were globally better for the two lowest xylose concentrations. It was checked at short reaction times, when the structural evolution of the catalyst can be supposed as negligible, whether the experimental initial reaction rates (calculated between t = 0 and 10 min) coincided with the model. For the lowest concentration, the agreement was excellent and the Ni-Fe catalyst was confirmed as the more active of the two by 25%. Differences between experiments and models appeared when the initial xylose concentration increased (the initial rate is underestimated by 30-40% for the highest xylose concentration), but the model satisfactorily reproduced two trends: the narrowing gap between the initial rates of the two catalysts when xylose concentration increased, and the slightly lower initial rate of the Ni-Fe catalyst for the highest xylose concentration, which could stem from the inhibition by xylose adsorption. Nevertheless, the benefit of using the Ni-Fe catalyst appears clearly when one looks at the whole progress of the reaction, as the conversion reached after 240 min is always higher than with the Ni catalyst, including for the highest xylose initial concentration.

Independent fitting of the three sets of measurements done with $Ni_{62}Fe_{38}/SiO_2$ led to values of k varying between 0.018 and 0.022 min^{-1}, that is, an error margin of 10% with respect to 0.020 min^{-1}. For measurements at the two lowest concentrations using Ni_{00}/SiO_2, k was confirmed at 0.013 min^{-1}, a value significantly below the range of k values determined for $Ni_{62}Fe_{38}/SiO_2$. But the value of k found for the highest concentration of xylose lay well below 0.013 min^{-1}, at 0.008 min^{-1}, and it can be easily seen from Figure 3 that the model based on equation (5) fails to describe the experiment correctly: the model departs from the experimental data after 60 min (Figure 3), and xylose conversion is much lower than what the model predicts. For this experiment, plotting 1/r as a function of 1 / C^{xylose} independently resulted in a negative adsorption constant. This contradiction suggests that the Ni catalyst properties deteriorate at long reaction time in these conditions.

The Ni_{100}/SiO_2 and $Ni_{62}Fe_{38}/SiO_2$ catalysts thus showed a high catalytic activity across the range of xylose concentration tested here (3.7-11.0 wt.%), at a temperature of 80 °C only, compared with other systems reported in the literature for which a lower xylose concentration (0.5-4.7 wt.%) and a higher reaction temperature (140-150 °C) were generally used.[31,34,35] Compared with the Ni catalyst, the specificity of bimetallic $Ni_{62}Fe_{38}/SiO_2$ seems to be related to a larger apparent rate constant (competing though with a larger adsorption constant of xylose on the active sites) and to a higher stability. Commenting on the origin of the differences between the apparent rate constants is difficult, as in this model, rate constants implicitly include contributions from the true kinetic constant, from adsorption constants, and from the number of active sites, all of which can differ between the two catalysts. Furthermore, the stability of the catalysts in reaction conditions needs to be taken into account and will be investigated in more detail in the last section.

Shi et *al.* have summarized the possible roles of iron in promoting the adsorption and reactivity of oxygenates (aldehydes, ketones, furanic compounds, acids, esters, monosaccharides) during hydrogenation on Ni-Fe catalysts.[44] The first effect is electronic. Fe being a more electropositive metal compared to Ni, a charge transfer from Fe to Ni can take place on Ni-Fe particles, with an increase of electron density on Ni leading to strengthened metal–carbon bonding, and to the activation of the adsorbed oxygen-containing function by bond weakening. The second effect is linked to the oxophilicity of Fe with respect to Ni. A dual role has been assigned, on the one hand to Fe for the optimal adsorption of the oxygen atom from the polar function, and on the other hand to Ni for the activation of the CO function and adsorption of H_2. Effects of Fe both on the adsorption of xylose and on the kinetics of the rate-determining steps of xylose hydrogenation can thus derive from the promotion by Fe.

We verified to which extent $Ni_{62}Fe_{38}/SiO_2$ benefits from the presence of Fe in a reduced form. An experiment was carried out on a $Ni_{62}Fe_{38}/SiO_2$ catalyst that was reduced at 400 °C only after DPU, without pre-reduction at 700 °C. It was formerly shown that at 400 °C, particles mainly consist of a reduced Ni-rich core surrounded by Fe(II) oxidic species.[37] The Ni-Fe catalyst on which iron is oxidized is less active than the catalyst pre-reduced at 700 °C (**Erreur ! Source du renvoi introuvable.**). Values of $k = 0.018$ min^{-1} and $K = 9.3$ $L.mol^{-1}$ were found to model the progress of the reaction for the catalyst reduced at 400 °C. Reducing

Fe to the metallic state, as is done by the initial reduction step at 700°C, would thus improve the catalyst properties by diminishing the magnitude of the inhibiting term.

We finally checked how the rate law could be approximated by an equation based on an apparent order n with respect to xylose, $v = k_{app} (C^{xylose})^n$. With 3.7 wt.% xylose, n was found to be equal to 0.95 for Ni_{100}/SiO_2 and 0.85 for $Ni_{62}Fe_{38}/SiO_2$. The initial first-order hypothesis was thus correct for Ni owing to the small value of K, but represented a significant approximation for Ni-Fe. Comparison with **Erreur ! Source du renvoi introuvable.** shows that the rate constant determined using a first-order hypothesis was underestimated by 15% with respect to the model exhibiting the inhibiting term. The value of Ea calculated above, and based on the first-order hypothesis, should thus be interpreted with care.

Table 1: Effect of xylose concentration on metal leaching (measured by ICP on the solutions), and conversion after 240 min of reaction. Reaction conditions: 20 bar H_2, 80 °C, 108 mg catalyst.

	Ni_{100}/SiO_2			$Ni_{62}Fe_{38}/SiO_2$			
	Leaching (ppm)			Leaching (ppm)			
C^{xylose} (wt.%)	Ni	Si	Conv. [%]	Ni	Fe	Si	Conv. [%]
3.7	12	124	94	7	15	111	100
7.3	24	130	92	14	68	107	99
11.0	31	115	77	15	62	103	91

For each of the six experiments, an ICP analysis was performed on the recovered solutions after 240 min of reaction (Table 1, which also mentions the conversion reached at 240 min). Ni_{100}/SiO_2 provided a significantly lower conversion of xylose whatever the initial concentration. The leaching of Si from the two catalysts was similar. The total amount of leached metals was higher for the bimetallic catalyst and increased with the xylose concentration. But, more specifically, the leaching of Ni from Ni_{100}/SiO_2 (12, 24, and 31 ppm) was almost twice larger than that from $Ni_{62}Fe_{38}/SiO_2$ (7, 14, and 15 ppm). In other terms, it is iron leaching that was predominant for $Ni_{62}Fe_{38}/SiO_2$, in agreement with the Fe enrichment in the outer shell of the alloyed nanoparticles. The lower loading of Ni on the bimetallic catalyst (about 40% of the metallic phase is iron) and the uneven distribution of the metals within the alloyed nanoparticles thus minimize the amount of Ni released in solution, without compromising the catalyst activity.

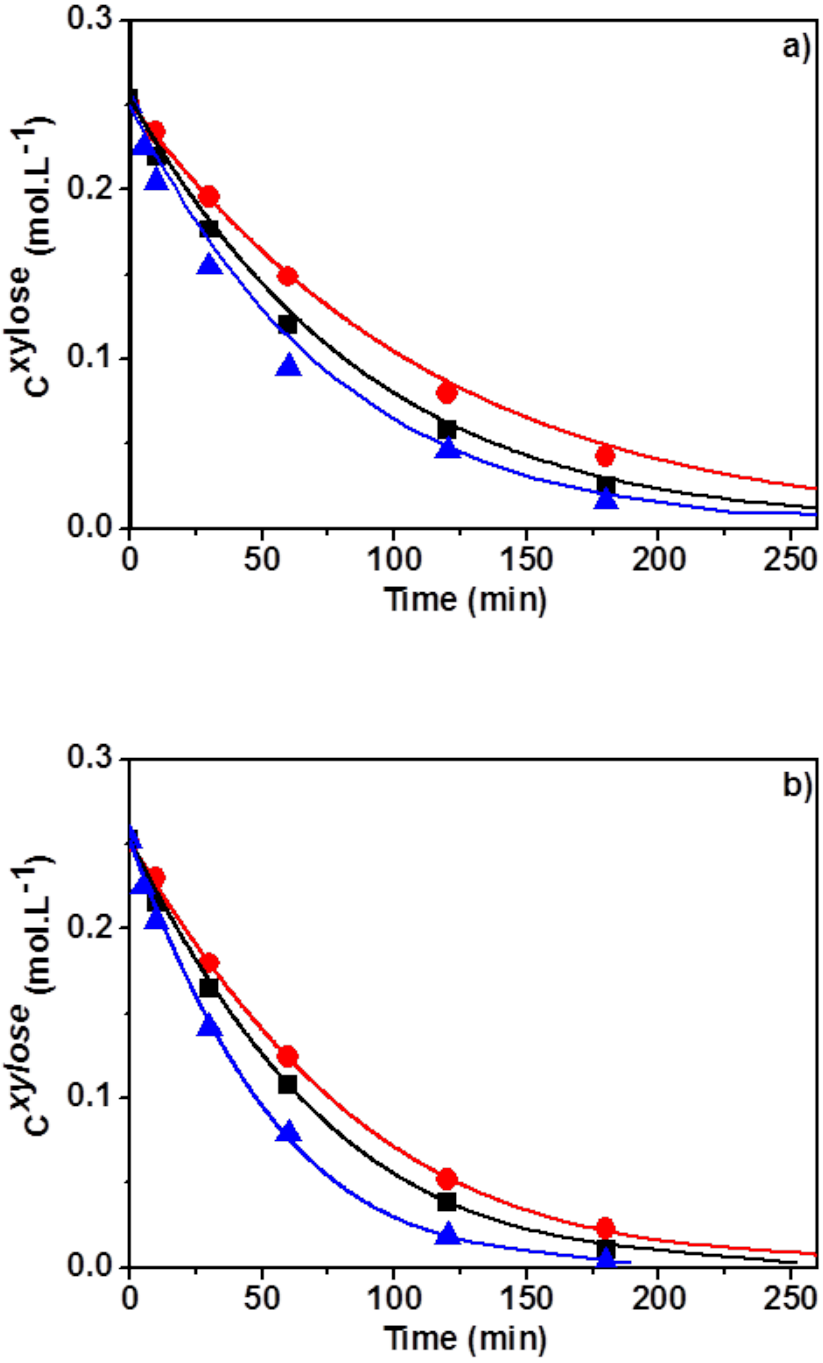

Figure 4: Evolution of xylose concentration as a function of time and hydrogen pressure over a) Ni_{100}/SiO_2 and b) $Ni_{62}Fe_{38}/SiO_2$ catalysts: (●) 10bar; (■) 20 bar; (▲) 30 bar. Reaction conditions: 3.7 wt.% xylose, 80 °C, 108 mg catalyst. Curves are calculated using the model based on equation (5).

The effect of H_2 pressure (10-30 bar) was studied at 80 °C for a xylose concentration of 0.26 mol.L^{-1} (Figure 4). Xylitol was again obtained with selectivity higher than 98%. Equation 5 was used to determine the values of k for each pressure, using the adsorption constant formerly determined (K = 0.77 and 2.40 L.mol^{-1} for Ni_{00}/SiO_2 and $Ni_{62}Fe_{38}/SiO_2$, respectively; **Erreur ! Source du renvoi introuvable.**), and supposing that k is a simple function of $P_{H2}{}^m$. From a plot of ln(k) versus ln(P_{H2}) (**Erreur ! Source du renvoi introuvable.**), the reaction order m with respect to hydrogen pressure was found to be very close over Ni_{100}/SiO_2 and $Ni_{62}Fe_{38}/SiO_2$, 0.40 and 0.43, respectively; the main difference between the two catalysts thus lies on the way they interact with xylose. An order close to 0.5 may indicate that the rate-determining step corresponds to the reaction between adsorbed xylose and one adsorbed hydrogen atom resulting from the dissociative adsorption of H_2. The presence of P_{H2} in an independent inhibiting term is also possible, implying a non-competitive adsorption with respect to xylose.

Stability of Ni_{100}/SiO_2 and $Ni_{62}Fe_{38}/SiO_2$ catalysts in aqueous phase

In order to compare the stability of the two catalysts, recyclability tests were carried out for Ni_{100}/SiO_2 and $Ni_{62}Fe_{38}/SiO_2$ at 80 °C under 20 bar H_2 (Figure 5). A reaction time of 90 min was selected for each run in order to keep xylose conversion below 100%, while ensuring that the catalysts were exposed to the reaction conditions for a long time. The catalysts were collected by centrifugation after each run and dried overnight at 60°C. Re-activation of the catalysts was done under H_2 at 400 °C for 2 h before each run.

In the case of Ni_{100}/SiO_2 (Run 1), xylose conversion decreased in each successive run, and a conversion of only 25% was achieved during the third run. On the other hand, the catalytic activity remained stable for three runs of reaction in the presence of $Ni_{62}Fe_{38}/SiO_2$ (~72-74%). The carbon balance was higher than 98% during the recyclability tests over both catalysts and xylitol was the only detected product. Similar results were obtained at 50 °C after 480 min of reaction. $Ni_{62}Fe_{38}/SiO_2$ was stable for three runs (~69-71% conversion), whereas Ni_{100}/SiO_2 exhibited a decrease of catalytic activity (**Erreur ! Source du renvoi introuvable.**).

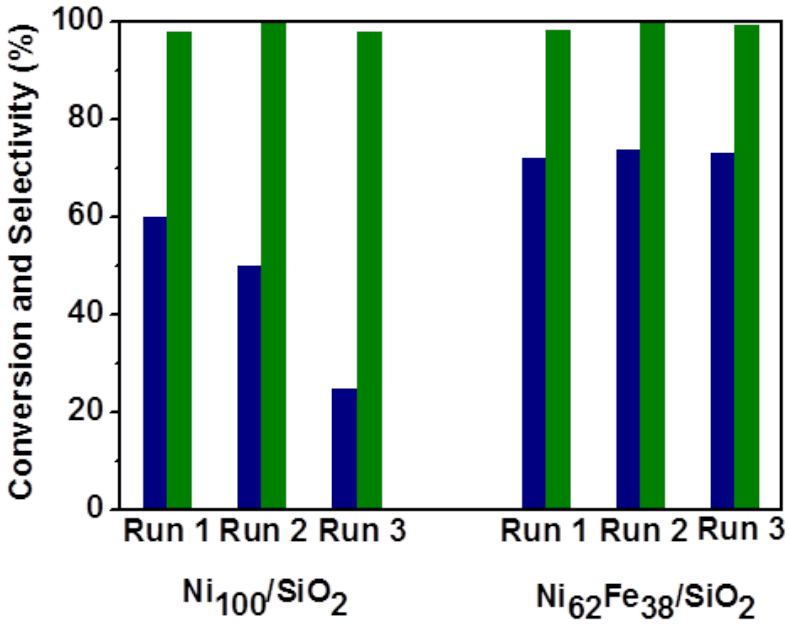

Figure 5: Catalyst recyclability study. (■) xylose conversion, (■) xylitol selectivity. Reaction conditions: 3.7 wt.% xylose , 20 bar H_2, 80 °C, 108 mg catalyst, reaction time = 90 min, n_{xylose}/n_{Ni} = 9.7, $n_{xylose}/n_{Ni}+n_{Fe}$ = 10.6.

The aqueous solutions were analyzed by ICP after each run at 80 °C in order to evaluate leaching. Leaching occurred primarily during the first run, and was less pronounced upon each subsequent run (Table 2). This low leaching of Ni thus does not explain the decrease in the catalytic activity observed upon recycling of the monometallic catalyst. Further characterization was performed to explain why the Ni catalyst deactivated.

Table 2: Metal leaching in the recyclability tests during the hydrogenation of xylose over Ni_{100}/SiO_2 and $Ni_{62}Fe_{38}/SiO_2$ catalysts. Reaction conditions: 3.7 wt.% xylose, 20 bar H_2, 80 °C, 108 mg catalyst, n_{xylose}/n_{Ni} = 9.7, $n_{xylose}/n_{Ni}+n_{Fe}$ = 10.6.

	Leaching by ICP (ppm)				
	Ni_{100}/SiO_2		$Ni_{62}Fe_{38}/SiO_2$		
	Ni	Si	Ni	Fe	Si
Run 1	12	124	7	15	111
Run 2	7	98	7	6	75
Run 3	6	68	2	5	63

A TGA analysis under air of the recycled catalysts was first done to evaluate the amount of adsorbed organic species after 3 runs. The mass loss assigned to the elimination of carbonaceous species between 100 and 400 °C amounted to 2 wt.% for the Ni catalyst and 7 wt.% for the Ni-Fe catalyst. This corresponds to less than 1% of the xylose introduced in solution for the three runs, in line with the high carbon balances calculated for each test. The lower amount of adsorbed species does not explain the deactivation of Ni_{100}/SiO_2.

The XRD patterns of the fresh catalysts and of the spent catalysts after three runs are presented in Figure 6. For the fresh Ni_{100}/SiO_2 catalyst, the diffraction peaks were assigned to metallic *fcc* Ni.[37] Two new diffraction peaks corresponding to a layered nickel hydroxide or phyllosilicate phase were observed at 2Θ = 34.7 and 60.5° for the spent Ni_{100}/SiO_2 catalyst. Lin *et al* suggested that the formation of $Ni(OH)_2$ deactivated a Ni/TiO_2 catalyst in the aqueous phase hydrogenation of nitrobenzene at 80 °C under 65 bar H_2.[45] The conversion of nitrobenzene after 6 h decreased from 80% to less than 10% in the second run. Diffraction peaks assigned to the bimetallic *fcc* Ni-Fe alloy were visible on the diffractogram of the fresh $Ni_{62}Fe_{38}/SiO_2$ catalyst.[37] Two new diffraction peaks assigned to nickel layered hydrated phases were observed for the spent catalyst, but with a low intensity compared with the Ni catalyst.

TEM images confirm that spent Ni_{100}/SiO_2 was much more damaged by the reaction conditions than $Ni_{62}Fe_{38}/SiO_2$ (**Erreur ! Source du renvoi introuvable.**, **Erreur ! Source du renvoi introuvable.**). Some catalyst grains fully converted to layered phases containing nickel (II), as proved by EDX measurements, with reduced metal particles completely disappearing from these zones (**Erreur ! Source du renvoi introuvable.**b). This loss of metallic nickel by transformation of the catalyst during reaction may challenge the possibility to apply a simple kinetic model to Ni_{100}/SiO_2 over the whole course of the reaction, and explain why the model presented above failed to correctly describe the whole set of catalytic measurements. In contrast, even if some small layered zones are visible on **Erreur ! Source du renvoi introuvable.**b, the presence of iron in the alloyed particles seems to preserve the overall morphology of the $Ni_{62}Fe_{38}/SiO_2$ catalyst to a larger extent.

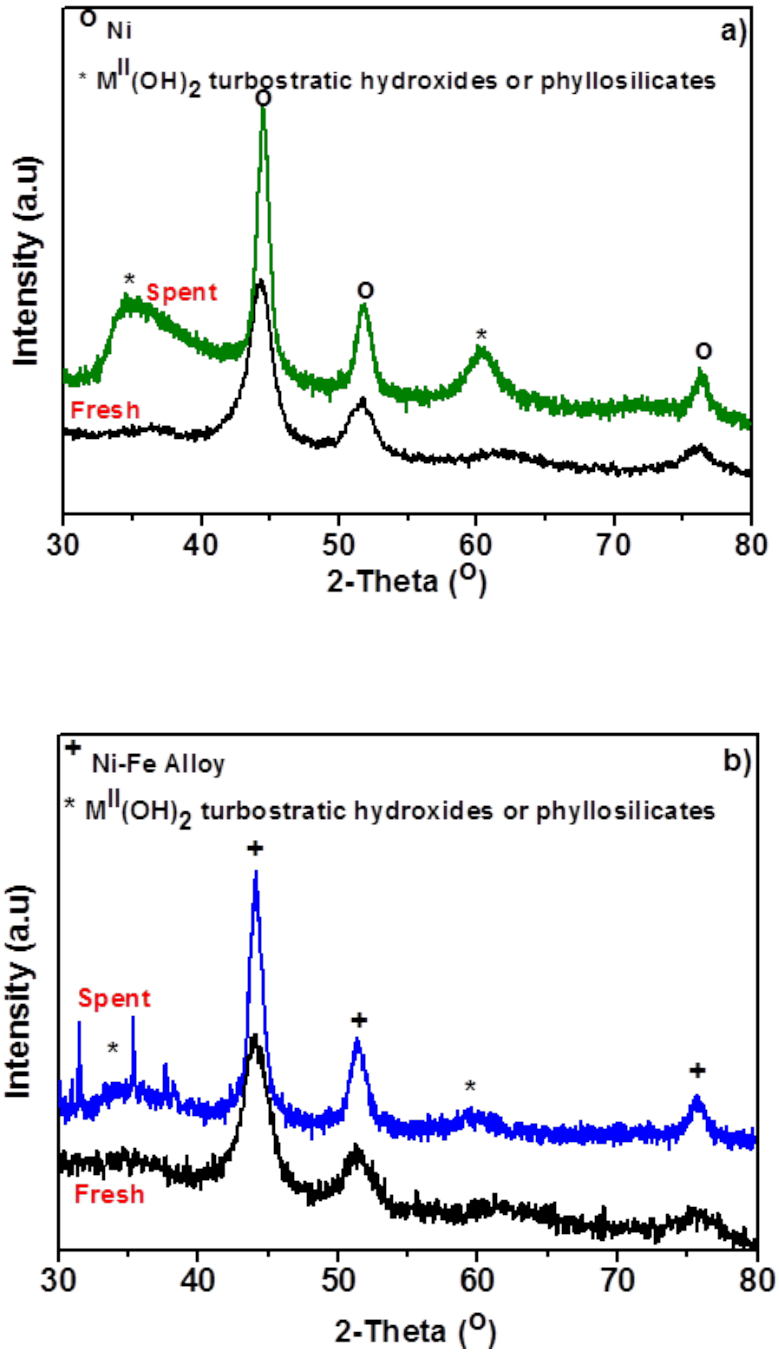

Figure 6: XRD patterns of a) Ni_{100}/SiO_2, b) $Ni_{62}Fe_{38}/SiO_2$ catalysts after recyclability tests.

This increase of stability linked to the presence of a promoter within and at the surface of the Ni particles has been reported during the hydrogenation of xylose and glucose in water, at 140 °C, in the presence of Ni-Re/AC and Ni-Fe/CB catalysts.[31,35] An ICP analysis after the first run showed that the leaching of Ni for Ni-Re/AC (2.1%) was approximately one fifth of that of Ni/AC (10.2%).[31] Similarly, after the hydrogenation test, 10.8 % of Ni leached into the water medium was detected for the Ni/CB catalyst, while only 6.5 % of Ni was leached away from Ni-Fe/CB catalyst.[35]

However, further examination of the metal particles on $Ni_{62}Fe_{38}/SiO_2$ shows that the situation is not completely straightforward. The average particle size measured by TEM on $Ni_{62}Fe_{38}/SiO_2$ was found to increase from 5 nm in the fresh catalyst to 12 nm in the spent catalyst (**Erreur ! Source du renvoi introuvable.**), in accordance with the observed thinning of the XRD peaks of the Ni-Fe particles (Figure 6). Similar sintering was reported for a Ni-Fe/CB catalyst used for glucose hydrogenation by Fu *et al.*[35]

LEIS spectroscopy was selected to investigate possible changes of atomic composition within the outermost layers of the bimetallic nanoparticles, as, unlike X-ray photoelectron spectroscopy which globally probes a thickness of a few nanometers, LEIS is more sensitive to the first atomic layers. LEIS measurements were carried out after an activation of the catalysts in H_2 at 400°C. Figure 7 presents the decomposition of the LEIS spectra of fresh and spent $Ni_{62}Fe_{38}/SiO_2$, after background subtraction (for more information, the evolution of the LEIS Fe/Ni atomic ratio as a function of the total ionic dose is shown on **Erreur ! Source du renvoi introuvable.**). The Fe/Ni atomic ratio was calculated as 1.2 ± 0.2 on the fresh catalyst, confirming the existence of a Fe-rich shell evidenced by other techniques.[37] This ratio increased to 3.4 ± 0.2 on the spent catalyst at ionic iso-dose, revealing a further increase of Fe at the surface of the bimetallic particles.

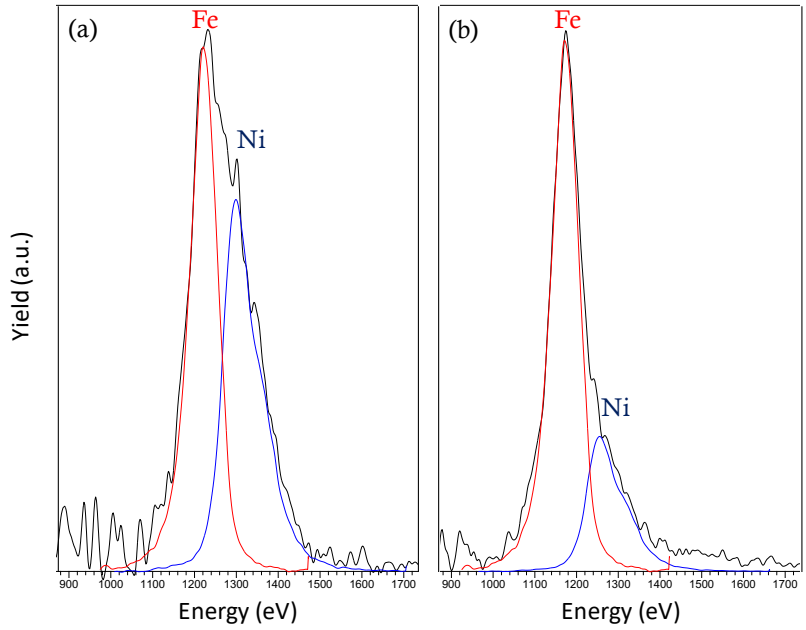

Figure 7: Decomposition of the LEIS spectra of a) fresh $Ni_{62}Fe_{38}/SiO_2$ and b) spent $Ni_{62}Fe_{38}/SiO_2$ at a total ionic dose of 1.4 x 10^{16} ions.cm^2 (5 keV Ne^+).

Even if the catalytic activity is not compromised, these results show that a restructuring of the Ni-Fe nanoparticles takes place, both in terms of particle size and metal distribution. The increase of the particle size observed by TEM (measurements performed on samples stored in air, no prior activation in H_2) may be ascribed in part to the deeper oxidation of the spent particles whose outer part has become enriched in Fe, a metal more sensitive than nickel to oxidation in air. A flattening and coalescing of the Ni-Fe particles over the surface of silica can explain the TEM and LEIS observations, and it is the presence of an expanded Fe-rich shell that would block the total conversion of the particles to phyllosilicate seen for Ni. We believe that the validity of the kinetic model presented above still holds for a comparison of the catalysts, because of the agreement between the experimental data and the model at short reaction time. However, the restructuring of the catalyst makes a general interpretation challenging and should be taken in consideration for further studies. The retention of the catalytic activity, despite the relative decrease of Ni from the catalyst surface, also raises questions about the exact nature and number of the active sites on the fresh and restructured Ni-Fe nanoparticles, and perhaps on the moment these sites form in reaction conditions.

Conclusion

The benefit of promoting Ni with reduced Fe in alloyed Ni-Fe nanoparticles was investigated for the aqueous phase hydrogenation of xylose by comparing two SiO_2-supported catalysts prepared by deposition-precipitation with urea, and exhibiting the same characteristics in terms of particle size. Whatever the reaction conditions and the catalyst, the only product detected was xylitol, with selectivity and carbon balance higher than 98%. Between 50 and 125 °C, the Ni-Fe catalyst was found to be more active than its Ni homologue. A minimal leaching of the metals, in particular that of Ni, was measured for a reaction temperature of 80 °C. A kinetic model featuring xylose concentration in the inhibiting term of the rate law was shown to describe the evolution of the conversion with time for the Ni-Fe catalyst, for initial mass fractions of xylose in water ranging from 3.7 to 11.0 wt.%. The Ni-Fe catalyst showed a higher stability of its catalytic properties compared with the monometallic Ni catalyst, which exhibited a decrease of catalytic activity upon successive runs, associated to a pronounced conversion to a hydrated Ni^{2+}-phyllosilicate phase in the reaction conditions. The benefits of using Fe as a promoter of Ni for the aqueous phase hydrogenation of xylose can thus be found at two levels: increasing the catalyst activity, presumably through the involvement of reduced Fe in the adsorption of xylose, and maintaining the catalytic activity by increasing the chemical stability of the catalyst. However, interpreting the properties of the Ni-Fe catalyst is not straightforward, as the Ni-Fe nanoparticles undergo some restructuration under reaction: increase of the particle size and of the proportion of Fe in the upper atomic layers, which may be explained by a flattening and coalescing of the particles over silica.

Acknowledgements

The financial support of this work was provided by the French National Research Agency (ANR), through the NobleFreeCat project (ANR-17-CE07-0022). The authors acknowledge the scientific services of Centrale Lille: Joelle Thuriot-Roukos (ICP), Svetlana Heyte (SPR/HPLC); and the help of Olivier Gardoll and Pardis Simon (UCCS) for the TGA measurements and for the set-up of the environmental cell for activation prior to LEIS measurements, respectively. The Chevreul Institute is thanked for its help in the development of this work through the ARCHI-CM project supported by the “Ministère de l’Enseignement

Supérieur de la Recherche et de l'Innovation", the region "Hauts-de-France", the ERDF program of the European Union and the "Métropole Européenne de Lille". The authors would like to thank Mr. Ahmed Addad for his help in carrying out the work on the electron microscopy facility of the Advanced Characterization Platform of the Chevreul Institute.
The REALCAT platform is benefitting from a state subsidy administrated by the French National Research Agency (ANR) within the frame of the 'Future Investments' program (PIA), with the contractual reference 'ANR-11-EQPX-0037'. The European Union, through the ERDF funding administered by the Hauts-de-France Region, has co-financed the platform. Centrale Lille, the CNRS, and University of Lille as well as the Centrale Initiatives Foundation, are thanked for their financial contributions to the acquisition and implementation of the equipment.

References:

[1] J. C. Serrano-Ruiz, R. Luque, A. Sepúlveda-Escribano, *Chem. Soc. Rev.* **2011**, *40*, 5266–5281.
[2] M. Besson, P. Gallezot, C. Pinel, *Chem. Rev.* **2014**, *114*, 1827–1870.
[3] D. M. Alonso, J. Q. Bond, J. A. Dumesic, *Green Chem.* **2010**, *12*, 1493–1513.
[4] J. S. Luterbacher, D. Martin Alonso, J. A. Dumesic, *Green Chem* **2014**, *16*, 4816–4838.
[5] A. M. Ruppert, K. Weinberg, R. Palkovits, *Angew. Chem. Int. Ed.* **2012**, *51*, 2564–2601.
[6] A. P. Tathod, P. L. Dhepe, *Green Chem* **2014**, *16*, 4944–4954.
[7] J. E. Holladay, J. J. Bozell, J. F. White, D. Johnson, *DOE Rep. PNNL* **2007**, *16983*.
[8] L. Venkateswar Rao, J. K. Goli, J. Gentela, S. Koti, *Bioresour. Technol.* **2016**, *213*, 299–310.
[9] M. Yadav, D. K. Mishra, J.-S. Hwang, *Appl. Catal. Gen.* **2012**, *425–426*, 110–116.
[10] B. Zada, M. Chen, C. Chen, L. Yan, Q. Xu, W. Li, Q. Guo, Y. Fu, *Sci. China Chem.* **2017**, *60*, 853–869.
[11] C. Hayes, *J. Dent. Educ.* **2001**, *65*, 1106–1109.
[12] M. G. Marmot, M. J. Shipley, *Bmj* **1996**, *313*, 1180–1184.
[13] R. Pulicharla, L. Lonappan, S. K. Brar, M. Verma, in *Platf. Chem. Biorefinery*, Elsevier, Amsterdam, Netherlands, **2016**, pp. 201–216.
[14] A. Sokmen, G. Gunes, *LWT - Food Sci. Technol.* **2006**, *39*, 1053–1058.
[15] Y. Delgado Arcaño, O. D. Valmaña García, D. Mandelli, W. A. Carvalho, L. A. Magalhães Pontes, *Catal. Today* **2020**, *344*, 2–14.
[16] B. W. Hoffer, E. Crezee, P. R. M. Mooijman, A. D. van Langeveld, F. Kapteijn, J. A. Moulijn, *Catal. Today* **2003**, *79–80*, 35–41.
[17] B. Kusserow, S. Schimpf, P. Claus, *Adv. Synth. Catal.* **2003**, *345*, 289–299.
[18] J. Pan, J. Li, C. Wang, Z. Yang, *React. Kinet. Catal. Lett.* **2007**, *90*, 233–242.
[19] P. Gallezot, N. Nicolaus, G. Fl`eche, P. Fuertes, A. Perrard, *J. Catal.* **1998**, *180*, 51–55.
[20] M. Audemar, W. Ramdani, T. Junhui, A. Raluca Ifrim, A. Ungureanu, F. Jérôme, S. Royer, K. Oliveira Vigier, *ChemCatChem* **2020**, *12*, 1973–1978.
[21] T. Deng, G. Xu, Y. Fu, *Chin. J. Catal.* **2020**, *41*, 404–414.

[22] J. Wisniak, M. Hershkowitz, R. Leibowitz, S. Stein, *Ind. Eng. Chem. Prod. Res. Dev.* **1974**, *13*, 75–79.
[23] K. Jyrki, H. Heikki, T. Matti, G. Martin, R. Teppo, *Hydrogenation Process for the Production of a Sugar Alcohol*, **2014**, US 8,816,068.
[24] H. Heikkilä, R. Alen, S. Kauko, M. Lindroos, J. Nurmi, P. Sarmala, M. Tylli, *Method of Producing Polyols from Arabinoxylan-Containing Material*, **2001**, US 6,262,318 B1.
[25] J.-P. Mikkola, T. Salmi, *Chem. Eng. Sci.* **1999**, *54*, 1583–1588.
[26] R. Geyer, P. Kraak, A. Pachulski, R. Schödel, *Chem. Ing. Tech.* **2012**, *84*, 513–516.
[27] B. Hoffer, *Appl. Catal. Gen.* **2003**, *253*, 437–452.
[28] P. Gallezot, P. J. Cerino, B. Blanc, G. Fleche, P. Fuertes, *J. Catal.* **1994**, *146*, 93–102.
[29] A. Corma, S. Iborra, A. Velty, *Chem. Rev.* **2007**, *107*, 2411–2502.
[30] J.-P. Mikkola, R. Sjöholm, T. Salmi, P. Mäki-Arvela, *Catal. Today* **1999**, *48*, 73–81.
[31] H. Xia, L. Zhang, H. Hu, S. Zuo, L. Yang, *Nanomaterials* **2019**, *10*, 73–86.
[32] J. Pang, A. Wang, M. Zheng, Y. Zhang, Y. Huang, X. Chen, T. Zhang, *Green Chem.* **2012**, *14*, 614–617.
[33] G. Liang, L. He, M. Arai, F. Zhao, *ChemSusChem* **2014**, *7*, 1415–1421.
[34] G. Chieffi, C. Giordano, M. Antonietti, D. Esposito, *J. Mater. Chem. A* **2014**, *2*, 11591–11596.
[35] Y. Fu, L. Ding, M. L. Singleton, H. Idrissi, S. Hermans, *Appl. Catal. B Environ.* **2021**, *288*, 119997.
[36] I. McDonald, G. C. Sloan, A. A. Zijlstra, N. Matsunaga, M. Matsuura, K. E. Kraemer, J. Bernard-Salas, A. J. Markwick, *Astrophys. J.* **2010**, *717*, L92–L97.
[37] D. Shi, Q. Yang, C. Peterson, A.-F. Lamic-Humblot, J.-S. Girardon, A. Griboval-Constant, L. Stievano, M. T. Sougrati, V. Briois, P. A. J. Bagot, R. Wojcieszak, S. Paul, E. Marceau, *Catal. Today* **2019**, *334*, 162–172.
[38] V. S. Chernysh, H. H. Brongersma, P. Brüner, T. Grehl, *Nucl. Instrum. Methods Phys. Res. Sect. B Beam Interact. Mater. At.* **2019**, *460*, 180–184.
[39] E. Symianakis, D. Malko, E. Ahmad, A.-S. Mamede, J.-F. Paul, N. Harrison, A. Kucernak, *J. Phys. Chem. C* **2015**, *119*, 12209–12217.
[40] H. Brongersma, M. Draxler, M. Deridder, P. Bauer, *Surf. Sci. Rep.* **2007**, *62*, 63–109.
[41] T. N. Pham, A. Samikannu, A.-R. Rautio, K. L. Juhasz, Z. Konya, J. Wärnå, K. Kordas, J.-P. Mikkola, *Top. Catal.* **2016**, *59*, 1165–1177.
[42] J.-P. Mikkola, H. Vainio, T. Salmi, R. Sjöholm, T. Ollonqvist, J. Väyrynen, *Appl. Catal. Gen.* **2000**, *196*, 143–155.
[43] D. K. Mishra, A. A. Dabbawala, J.-S. Hwang, *J. Mol. Catal. Chem.* **2013**, *376*, 63–70.
[44] D. Shi, R. Wojcieszak, S. Paul, E. Marceau, *Catalysts* **2019**, *9*, 451.
[45] W. Lin, H. Cheng, J. Ming, Y. Yu, F. Zhao, *J. Catal.* **2012**, *291*, 149–154.